Nanotechnology **20** (2009) 125402 (13pp) doi:10.1088/0957-4484/20/12/125402

Thermoelectromechanical effects in quantum dots

Sunil R Patil and Roderick V N Melnik

M^{2}NeT Laboratory, Wilfrid Laurier University, 75 University Avenue West, Waterloo, ON, N2L 3C5, Canada

E-mail: spatil@wlu.ca and rmelnik@wlu.ca

Received 28 November 2008, in final form 16 January 2009
Published 3 March 2009
Online at stacks.iop.org/Nano/20/125402

Abstract

Electromechanical effects are important in semiconductor nanostructures as most of the semiconductors are piezoelectric in nature. These nanostructures find applications in electronic and optoelectronic devices where they may face challenges for thermal management. Low dimensional semiconductor nanostructures, such as quantum dots (QD) and nanowires, are the nanostructures where such challenges must be particularly carefully addressed. In this contribution we report a study on thermoelectromechanical effects in QDs. For the first time a coupled model of thermoelectroelasticity has been applied to the analysis of quantum dots and the influence of thermoelectromechanical effects on bandstructures of low dimensional nanostructures has been quantified. Finite element solutions are obtained for different thermal loadings and their effects on the electromechanical properties and bandstructure of QDs are presented. Our model accounts for a practically important range of internal and external thermoelectromechanical loadings. Results are obtained for typical QD systems based on GaN/AlN and CdSe/CdS (as representatives of III–V and II–VI group semiconductors, respectively), with cylindrical and truncated conical geometries. The wetting layer effect on electromechanical quantities is also accounted for. The energy bandstructure calculations for various thermal loadings are performed. Electromechanical fields are observed to be more sensitive to thermal loadings in GaN/AlN QDs as compared to CdSe/CdS QDs. The results are discussed in the context of the effect of thermal loadings on the performance of QD-based nanosystems.

(Some figures in this article are in colour only in the electronic version)

1. Introduction

Spatially confined motion of electrons in low dimensional semiconductor nanostructures (LDSNs) is attracting increasing attention of physics and engineering communities due to their current and potential applications in optoelectronics, biotechnology and other areas. LDSNs are strained structures as they are normally embedded in a host material with different structural properties. Piezoelectric effects in LDSNs are also important due to the fact that most of the semiconductor materials are piezoelectric in nature [1, 2]. Strain [3, 4] and piezoelectric effects [5] are being used as tuning parameters for the optical response of LDSNs in band gap engineering. On the other hand, thermal effects coupled with electric [6–13] and mechanical [14] fields in LDSNs have also become important. Indeed, as thermoelectric and thermoelastic effects are often significant in LDSNs [6, 13, 14], it is reasonable to expect that the temperature may also be used as a tuning parameter in band gap engineering [12, 13]. One of the difficulties related to this lies with the fact that the novel LDSN-based electronic and optoelectronic devices may face challenges for thermal management [6]. It is expected that by integrating LDSN materials into critical regions of microelectronic circuits, the excess heat that limits device performance will be effectively removed [7]. Therefore, a systematic study on thermal loadings is required for analyzing and optimizing their effects on optoelectronic properties of LDSNs. Furthermore, since there are many practical situations where the interaction of thermopiezoelectric structures with other media such as acoustic [15] and gas/fluid [16] needs to be accounted for, the present formulation can act as a foundation for the study of such coupled models in the context of LDSNs.

Our major attention in this paper is given to QDs, the nanostructures that are considered to be a basis for many innovatory nanoelectronic/optoelectronic devices [2], where thermal effects may also become important. This includes applications of QDs in low temperature Peltier refrigeration [17] and thermal rectifiers [18] as well as their applications for higher temperature ranges. Without accounting for the thermal field, both linear and nonlinear electromechanical effects in QDs and their influence on bandstructures are now better understood [1, 19–21]. Earlier studies have been focusing on coupled thermoelectric effect contributions at the device level based on energy balance models, generalizing drift–diffusion models and allowing us to account for non-local and non-equilibrium processes [22–25]. More recently, generalizations of drift–diffusion models have been carried out to account for quantum effects in LDSNs [26, 27]. At the same time, recent studies have been devoted to elucidating the importance of thermal effects in LDSNs, including the temperature induced stress resulting in phase transitions [28] as well as temperature-dependent phase stability [29] in nanostructures. Although the study of fully coupled thermoelectromechanical effects in QDs has both technological as well as fundamental interest, it has not been carried out until now.

In this paper, we present a mathematical model describing coupled thermoelectromechanical effects in LDSNs, its special cases and generalizations. Our particular focus is on the influence of thermoelectromechanical effects on properties of QDs. Furthermore, a major focus is given to GaN/AlN and CdSe/CdS QD systems, as representatives of III–V and II–VI group semiconductors, respectively. These semiconductors are wurtzite (WZ) crystals and the former ones (GaN-based) are known as potentially important thermoelectric materials [13]. In our study we take a sufficiently wide range of thermal loadings of our structures, from 0 to 1000 K, keeping in mind their potential applications as thermoelectrics and their operations in various temperature regimes. It is for this entire range of thermal loadings that the influence on electromechanical fields and energy bandstructures is studied. To be closer to realistic experimental setups, the geometries and dimensions used in this study are similar to those of experimentally grown QDs [30]. We also account for the wetting layer (WL) because a conventional analysis of QD structures without accounting for the WL may not be sufficient for an adequate characterization of QDs [31–33].

The paper is organized as follows. Section 2 provides details of the theoretical formulation of the fully coupled thermoelectromechanical problem for QDs along with constitutive equations and the explicit form of corresponding expressions for the wurtzite crystals we focus on. In section 3, the results of our study of the influence of thermal effects on the electromechanical behavior of QDs and the energy bandstructure, obtained with an 8-band $\mathbf{k}\cdot\mathbf{p}$ model, for QDs are presented. Section 4 highlights major conclusions drawn from this study.

2. Theory

In what follows, we formulate a mathematical model in order to study thermoelectromechanical effects in QDs. A general two-dimensional (2D) axisymmetric model is developed with coupled multi-physics governing equations. The model is based on a coupled system of equilibrium equations of elasticity, electrostatics and heat transfer.

2.1. Coupled system of equations for mechanical, electric and thermal fields

The linear fundamental equations for the thermoelectromechanical structure occupying volume Ω, under steady state conditions, can be summarized as follows [34, 35]:

mechanical equilibrium equation,

$$\sigma_{ij,j} + f_i = 0, \tag{1}$$

the equation of electrostatics,

$$D_{i,i} - q = 0, \tag{2}$$

the thermal energy balance equation,

$$h_{i,i} - k = 0. \tag{3}$$

Here σ_{ij} are stress tensor components, D_i are electric displacement vector components, h_i are the components of the heat flux vector, and f_i, q and k are body mechanical forces, electric charge and heat source in Ω, respectively. Coupling of equations (1)–(3) is implemented through constitutive equations described in section 2.3.

2.2. Gradient equations

Gradient equations correspond to the relationships between the linear strain and mechanical displacement, the electric field and electric potential, and the thermal field and temperature change. They are stated respectively as,

$$\varepsilon_{kl} = \tfrac{1}{2}(u_{k,l} + u_{l,k}), \tag{4}$$

$$E_k = -V_{,k}, \tag{5}$$

$$Q_k = -\Theta_{,k}, \tag{6}$$

where ε_{kl}, E_k, Q_k, u, V and Θ are the components of the strain tensor, electric field vector, thermal field vector, mechanical displacement vector, electric potential and temperature change from the reference, respectively. In section 2.5, we will extend equation (4) to account for lattice mismatch in typical nanostructures.

2.3. Constitutive equations

The (Helmholtz) free energy function, accounting for three independent variables, ε, E, and Θ, for our system has the following form:

$$\phi(\varepsilon_{ij}, E_i, \Theta) = \tfrac{1}{2}c_{ijkl}\varepsilon_{ij}\varepsilon_{kl} - e_{ijk}E_i\varepsilon_{jk} - \tfrac{1}{2}\in_{ij} E_iE_j - \beta_{ij}\Theta\varepsilon_{ij} - p_iE_i\Theta - \tfrac{1}{2}a_T\Theta^2, \tag{7}$$

where $a_T = c_\varepsilon^V / T_0$, and c_ε^V is the heat capacity at constant strain and electric field. The constitute relationships are derived from (7) as

$$\sigma_{ij} = \partial\phi/\partial\varepsilon_{ij}, \qquad D_i = -\partial\phi/\partial E_i, \qquad S = -\partial\phi/\partial\Theta, \tag{8}$$

where S denotes entropy. These constitutive relations relating thermoelectromechanical quantities are expressed as,

$$\sigma_{ij} = c_{ijkl}\varepsilon_{kl} - e_{ijk}E_k - \beta_{ij}\Theta, \tag{9}$$

$$D_i = e_{ikl}\varepsilon_{kl} + \in_{ik} E_k + p_i\Theta + P_i^{\mathrm{sp}}, \tag{10}$$

$$S = \beta_{ij}\varepsilon_{ij} + p_i E_i + a_T\Theta, \tag{11}$$

where c_{ijkl}, e_{ijk} and $\in_{ik}$ are the elastic moduli, piezoelectric constants and dielectric constants, respectively. P_i^{sp} is the spontaneous polarization, and p_i and β_{ij} are thermoelectric and thermomechanical coupling constants, respectively. In this linear case, the thermoelectric coupling coefficient is connected to the pyroelectric coefficient defined via $\partial P_i^{\mathrm{sp}}/\partial\Theta$ and measured under constant ε and E.

2.4. Special cases and generalizations

The model (1)–(3), (4)–(6), (9)–(11) we are focusing on in this contribution covers several important special cases which are becoming increasingly important in applications of low dimensional nanostructures such as quantum dots and often analyzed separately:

- piezoelectric (or more generally electromechanical) models;
- thermoelectric models;
- thermomechanical models.

In what follows, we briefly provide details on each of these three important special cases.

2.4.1. Piezoelectric or electromechanical effects. Constitutive equations of the linear piezoelectricity have the following form:

$$\sigma_{ij} = c_{ijkl}\varepsilon_{kl} - e_{ijk}E_k, \tag{12}$$

$$D_i = e_{ijk}\varepsilon_{jk} + \in_{ij} E_j. \tag{13}$$

The well-posedness of the corresponding mathematical models in this and in more general cases was shown in [36, 37] (see also references therein), while the analysis of the special types of boundary conditions was carried out in [38].

Coupled models of piezoelectricity in a general setting were analyzed in [39–41]. In [1] the resulting models of piezoelectricity were coupled with the Schrodinger equation for electronic bandstructure analysis of low dimensional nanostructures. This has been extended further to account for higher order effects such as electrostriction in [42].

2.4.2. Thermoelectric effects. In this case constitutive equations are usually written in terms of the electric current density j_i^{el} and the heat flux h_i as

$$j_i^{\mathrm{el}} = \rho E_i - \rho S_b \Theta_{,i}\,, \tag{14}$$

$$h_i = -\rho S_b \Theta V_{,i} - (\kappa_{ij} + S_b^2\rho\Theta)\Theta_{,i}\,, \tag{15}$$

where ρ is the electric conductivity, κ is the thermal conductivity, and S_b is the Seebeck coefficient (in the general case, these coefficients are temperature dependent), where the thermoelectric figure of merit for isotropic materials is defined through these coefficients as $Z = \Theta\rho S_b^2/\kappa$ [43].

Such models of coupled thermoelectricity were studied in [44] in the device application context. The relation (15) generalizes Fourier's law to account for both Peltier and Thompson effects. The governing equations in this case are

$$j_{,i}^{\mathrm{el}} = 0, \qquad h_{i,i} - K = 0, \tag{16}$$

with $K = -\mathbf{j}^{\mathrm{el}} \cdot \nabla V$. Due to this latter term (that can be interpreted as 'convective'), the resulting nonlinear model is a generalization of conventional linear models, including a thermoelectric model accounting for the linear Seebeck effect [45] in which case we have $h_i = -\kappa_{ij}\Theta_{,j}$ and the coupling is effectively realized via the first equation in (16). For example, in the one-dimensional case, when no Peltier–Thompson effects are present, we have the relationship $-E + S_b\,\mathrm{d}\Theta/\mathrm{d}x = 0$ with the temperature-dependent Seebeck coefficient S_b which replaces (16) in this particular case.

2.4.3. Thermomechanical effects. Constitutive equations for the case of thermomechanical interactions follow directly from our representations (9)–(11) and details on the corresponding linear models, their generalizations, and numerical methodologies for their solutions can be found in [46–51].

2.4.4. Generalization to thermo-magneto-electromechanical problems. Finally, we mention that a straightforward generalization of our model (1)–(3), (4)–(6), (9)–(11) to account for the magnetic field follows from the following representation of the Helmholtz free energy function:

$$\Phi(\varepsilon_{ij}, E_n, \theta, B_p) = \phi(\varepsilon_{ij}, E_i, \Theta) + \tfrac{1}{2}\nu_{pq}B_pB_q - \pi_{pij}\varepsilon_{ij}B_p - \lambda_{pm}E_mB_p - \tau_pB_p\Theta. \tag{17}$$

The resulting constitutive equations in this case have the following form:

$$\sigma_{kl} = (\partial\Phi/\partial\varepsilon_{kl})_{E,B,\Theta} = c_{ijkl}\varepsilon_{ij} - e_{mkl}E_m - \pi_{pkl}B_p - \beta_{kl}\Theta, \tag{18}$$

$$D_n = -(\partial\Phi/\partial E_n)_{\varepsilon,B,\Theta} = e_{nij}\varepsilon_{ij} + \in_{mn} E_m + \lambda_{pn}B_p + p_n\Theta, \tag{19}$$

$$H_q = (\partial\Phi/\partial B_q)_{\varepsilon,E,\Theta} = -\pi_{qij}\varepsilon_{ij} - \lambda_{qm}E_m + \nu_{pq}B_p - \tau_q\Theta, \tag{20}$$

$$S = -(\partial\Phi/\partial\Theta)_{\varepsilon,E,B} = \beta_{ij}\varepsilon_{ij} + p_mE_m + \tau_pB_p + a_T\Theta, \tag{21}$$

where, π, λ and τ are the piezo-magnetic, electro-magnetic, thermo-magnetic coupling constants, respectively, whereas $\nu = 1/\mu$, μ is permeability. This model is used in [52] to study thermo-magneto-electro-elastic effects in nanowire superlattices. Another generalization has recently been developed in [1, 53] where nonlinear strain effects were taken into account.

Next, we provide the explicit expressions for the model we focus on in the case of cylindrical wurtzite nanostructures.

2.5. Explicit form of governing equations for WZ nanostructures in cylindrical co-ordinates

Governing equations for WZ structures in this case are axisymmetric, hence all the thermal, electric and mechanical field solutions are axisymmetric as well. Therefore, the original 3D problem can be reduced in this case to a simpler 2D problem [19]. The linearly independent elastic constants and piezoelectric constants in a crystal with WZ symmetry are given as [5, 57]

$$\begin{gathered} C_{1111} = C_{11}, \qquad C_{1122} = C_{12}, \qquad C_{1133} = C_{13}, \\ C_{3333} = C_{33}, \qquad C_{2323} = C_{44}, \\ C_{2121} = (C_{11} - C_{12})/2, \qquad e_{311} = e_{31}, \\ e_{333} = e_{33}, \qquad e_{113} = e_{15}, \qquad \beta_{11} = \beta_1, \\ \beta_{33} = \beta_3, \qquad \in_{11} = \in_1, \qquad \in_{33} = \in_3 . \end{gathered} \tag{22}$$

The electromechanical balance equations (1) and (2) in the cylindrical co-ordinates for the axisymmetric case take the following form [36]:

$$\frac{\partial \sigma_{rr}}{\partial r} + \frac{\partial \sigma_{rz}}{\partial z} + \frac{\sigma_{rr} - \sigma_{\theta\theta}}{r} = 0, \tag{23}$$

$$\frac{\partial \sigma_{rz}}{\partial r} + \frac{\partial \sigma_{zz}}{\partial z} + \frac{1}{r}\sigma_{rz} = 0, \tag{24}$$

$$\frac{\partial D_r}{\partial r} + \frac{\partial D_z}{\partial z} + \frac{1}{r} D_r = 0. \tag{25}$$

These equations are invariant with respect to rotations around the z axis, e.g. [57]; hence, solutions can be separated into a (r, z) part and a θ part, subject to adequate boundary conditions. The constitutive relations in equations (9) and (10) then take the following form for WZ nanostructures:

$$\begin{gathered} \sigma_{rr} = C_{11}\varepsilon_{rr} + C_{12}\varepsilon_{\theta\theta} + C_{13}\varepsilon_{zz} - e_{31}E_z - \beta_1\Theta, \\ \sigma_{rz} = C_{44}\varepsilon_{rz} - e_{15}E_r, \\ \sigma_{zz} = C_{13}\varepsilon_{rr} + C_{13}\varepsilon_{\theta\theta} + C_{33}\varepsilon_{zz} - e_{33}E_z - \beta_3\Theta, \\ D_r = e_{15}\varepsilon_{rz} + \in_1 E_r, \\ D_z = e_{31}\varepsilon_{rr} + e_{31}\varepsilon_{\theta\theta} + e_{33}\varepsilon_{zz} + \in_{33} E_z + p_3\Theta + P_z^{\mathrm{sp}}. \end{gathered} \tag{26}$$

To take into account the lattice mismatch, the strain tensor components in equation (4) take the following form:

$$\begin{gathered} \varepsilon_{rr} = \frac{\partial u_r}{\partial r} - \varepsilon_a^* \qquad \varepsilon_{zz} = \frac{\partial u_z}{\partial z} - \varepsilon_c^* \\ \varepsilon_{\theta\theta} = \frac{u_r}{r} - \varepsilon_a^* \qquad \varepsilon_{rz} = \frac{1}{2}\left(\frac{\partial u_r}{\partial z} + \frac{\partial u_z}{\partial r}\right), \end{gathered} \tag{27}$$

with $\varepsilon_a^* = \frac{a_m - a_{\mathrm{QD}}}{a_{\mathrm{QD}}}$ and $\varepsilon_c^* = \frac{c_m - c_{\mathrm{QD}}}{c_{\mathrm{QD}}}$ inside the QD. Quantities, a_m, c_m and a_{QD}, c_{QD} are the lattice constants of the matrix and the QD, respectively, while quantities, ε_a^* and ε_c^* are the local intrinsic strains (lattice mismatch) along the a and c directions, respectively. The directions a and c correspond to the shorter and longer dimensions of the unit cell of the WZ crystal, respectively. As the substrate is relatively large compared to the QD, we follow common practice to neglect lattice mismatch inside the matrix, i.e. $\varepsilon_a^* = \varepsilon_c^* = 0$ [2, 19, 21, 58, 59].

Here, we neglect the Seebeck effect due to the relatively smaller values of Seebeck coefficients for semiconductor materials of present interest, ~ -10 V K^{-1} [54, 55] and thermal equilibrium is assumed. Therefore, the temperature change becomes spatially independent, effectively leading to the determination of the solution of the equations (1) and (2) only. However, these equations are coupled via constitutive relations (9) and (10) [56].

2.6. Bandstructure calculations

In order to highlight further our point regarding the influence of thermoelectromechanical effects on optoelectronic properties, we analyze the bandstructure with an 8-band $\mathbf{k}\cdot\mathbf{p}$ model. We consider two conduction bands coupled with six valance bands including heavy-hole, light-hole and spin–orbit bands. The crystal-field splitting is also accounted for. Electron–hole states are the eigenstates of the 8-band envelope function equation:

$$H\Psi = E\Psi, \tag{28}$$

where H is the 8×8 matrix of the Hamiltonian, Ψ is the eight-component column of the envelope wavefunction and E is the energy. The Hamiltonian H can be written as

$$H = \begin{pmatrix} H_{\mathrm{e}}^{\mathrm{k}} + H_{\mathrm{e}}^{\varepsilon} + E_{\mathrm{c}} & & & 0 \\ & H_{\mathrm{h}}^{\mathrm{k}} + H_{\mathrm{h}}^{\varepsilon} + E_{\mathrm{v}} & & \\ & & H_{\mathrm{e}}^{\mathrm{k}} + H_{\mathrm{e}}^{\varepsilon} + E_{\mathrm{c}} & \\ 0 & & & H_{\mathrm{h}}^{\mathrm{k}} + H_{\mathrm{h}}^{\varepsilon} + E_{\mathrm{v}} \end{pmatrix} + eV. \tag{29}$$

Here, $H_{\mathrm{e}}^{\mathrm{k}}$ and $H_{\mathrm{e}}^{\varepsilon}$ are the kinetic and strain dependent parts of the electron Hamiltonian, respectively, whereas $H_{\mathrm{h}}^{\mathrm{k}}$ and $H_{\mathrm{h}}^{\varepsilon}$ are the 3×3 matrix of the kinetic and strain dependent parts (the spin–orbit interaction and crystal-field splitting terms are included) of the hole Hamiltonian, respectively. E_{c} and E_{v} are the energies of unstrained conduction- and valence-band edges, respectively, e is the absolute value of the electronic charge and V is the piezoelectric potential. The unstrained valance band edge of AlN at $T = 0$ K is taken as a reference. The strain dependent electron–hole part of the Hamiltonian, piezoelectric potential and energy band edges are temperature dependent.

The underlying algebraic eigenvalue problem that needs to be solved after discretizing equations (28) and (29) can lead to a number of non-trivial difficulties discussed in detail in [60, 61], while the variational formulations of equations (28) and (29), effectively used in our finite element method, can be found in [62]. We consider the temperature dependence of the band gap energy with the following relation,

$$E_{\mathrm{g}}(\Theta) = E_{\mathrm{g}}(0) - \frac{\alpha_\Theta \Theta^2}{\beta_\Theta + \Theta}, \tag{30}$$

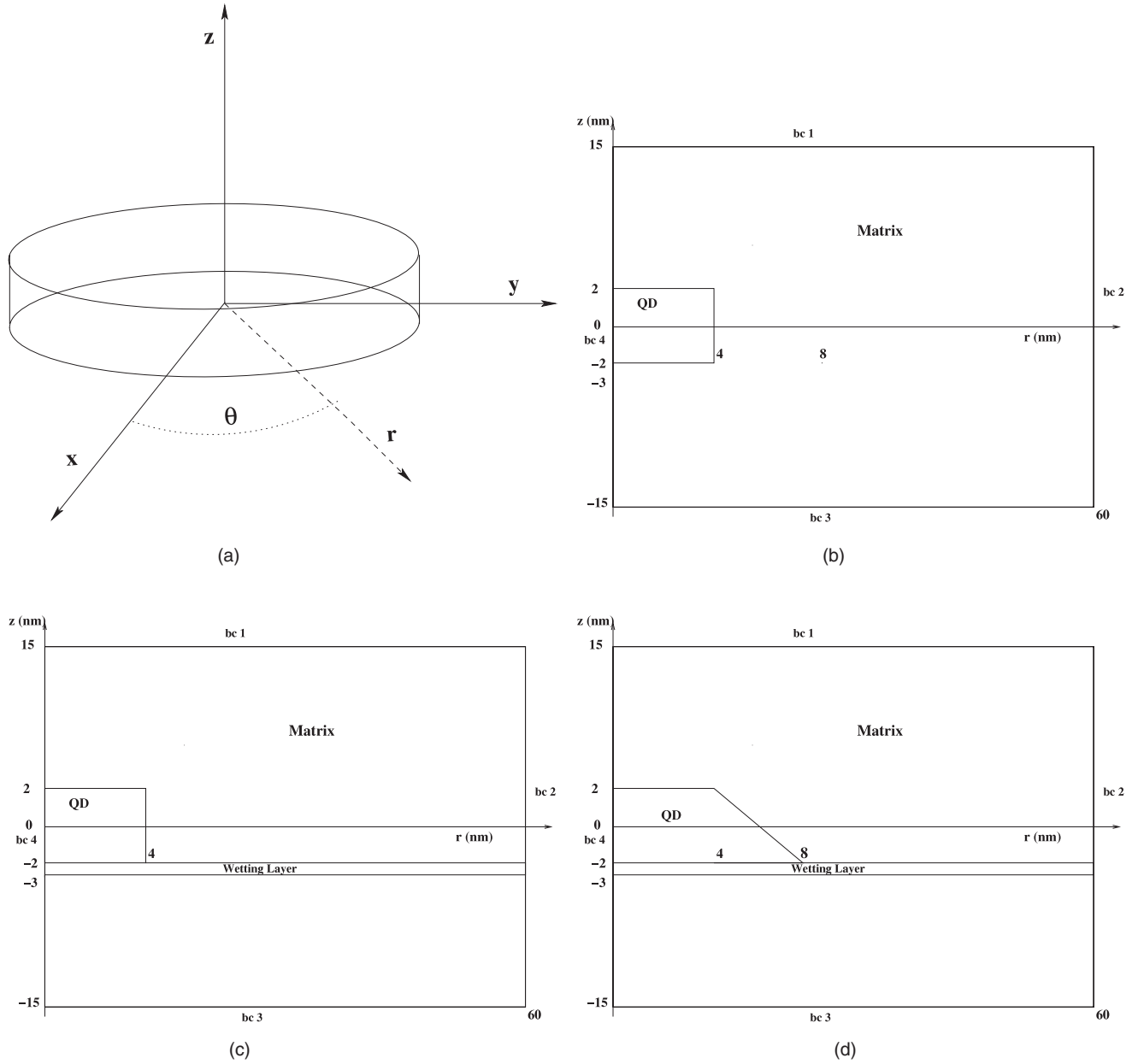

Figure 1. Geometry and co-ordinate system for the QD systems in the (r, z) plane. (a) Co-ordinate system, (b) cylindrical QD system, (c) cylindrical QD system with WL, (d) conical QD system with WL.

along with α_θ and β_θ as Varshni coefficients [63]. Further details of the expressions and parameters for the 8-band $\mathbf{k}\cdot\mathbf{p}$ Hamiltonian can be found in [5, 64, 65].

3. Results and discussions

Figure 1 shows the geometric details of the QD systems, where we consider three different cases with respect to geometries. The geometries we consider are: cylindrical without WL, cylindrical with WL, and truncated conical with WL. GaN/AlN and CdSe/CdS are the two different QD systems, which have been taken here for the analysis, as representatives of III–V and II–VI group semiconductors, respectively. Dirichlet boundary conditions are imposed along boundaries 1, 2, and 3 (see figure 1), while $u_r = 0$, $\frac{\partial u_z}{\partial r} = 0$, $\frac{\partial V}{\partial r} = 0$ and $\frac{\partial T}{\partial r} = 0$ at boundary 4 (denoted by bc4 in figure 1). Due to the axisymmetry of the system (equations, geometry and boundary conditions) there is no angular dependence.

The geometries and dimensions we consider here are based on experimental results (e.g. [30]), and the temperature range from 0 to 1000 K covers most thermoelectric applications of interest. As the deposition temperatures are normally above 1000 K [66, 67], we do not consider a special case of zero lattice mismatch inside QDs. We approximate experimentally grown (hexagonal) pyramidally shaped QDs [30] by truncating conical structures. This approximation can be made without significant error [20]. Physical parameters used in the calculations are given in

Table 1. Physical parameters of wurtzite GaN, AlN, CdSe and CdS.

Constants	GaN	AlN	CdSe	CdS
Stiffness coefficients (GPa)				
c_{11}	390 [73]	396 [73]	74.6 [74]	90.68 [56]
c_{12}	145 [73]	137 [73]	46.1 [74]	58.09 [56]
c_{13}	106 [73]	108 [73]	39.3 [75]	50.9 [56]
c_{33}	398 [73]	373 [73]	81.7 [74]	93.8 [56]
c_{44}	105 [73]	116 [73]	13.0 [74]	14.3 [76]
Permittivity				
Υ_{11}	9.28 [73]	8.67 [73]	9.29 [74]	8.28 [77]
Υ_{33}	10.01 [73]	8.57 [73]	10.16 [74]	8.73 [77]
Piezoelectric coefficients (C m^{-2})				
e_{15}	−0.49 [73]	−0.6 [73]	−0.138 [74]	−0.212 [78]
e_{31}	−0.49 [73]	−0.6 [73]	−0.16 [74]	−0.265 [78]
e_{33}	0.73 [73]	1.46 [73]	0.347 [74]	0.385 [78]
Pyroelectric coefficients (C m^{-2} K^{-1})				
$p_1 \times 10^{-6}$	0.91 [79]	7.5 [79]	−3.5 [80]	−4.0 [56, 80]
Thermal expansion coefficients (K^{-1})				
$\alpha \times 10^{-6}$				
α_a	5.57 [81]	4.2 [81]	4.13 [75]	4.3 [78]
α_c	3.17 [81]	5.3 [81]	2.76 [75]	2.77 [78]
Young's modulus E (GPa)	181 [82]	308 [83]	43.1 [78]	48.1 [78]
Poisson ratio ν	0.352 [82]	0.287 [84]	0.37 [78]	0.37 [78]
Spontaneous polarization P^{sp} (C m^{-2})	−0.029 [73]	−0.081 [73]	0.006 [85]	0.002 [85]
Lattice constant (Å)				
a	3.189 [73]	3.112 [73]	4.3 [78]	4.135 [78]
c	5.185 [73]	4.982 [73]	7.01 [78]	6.749 [78]
Stress–temperature coefficient (Pa K^{-1}) (Calculated using [86])				
$\beta_1 \times 10^5$	5.57	−4.44	1.1	−0.98
$\beta_3 \times 10^5$	−8.66	6.9	−0.13	0.116

Table 2. Magnitudes of energy band gap related parameters for wurtzite GaN and AlN.

Bandstructure parameters	GaN	AlN
E_g (eV) [5]	3.475	6.23
$a_c^{\perp}$ (eV) [5]	−8.2	−5.4
$a_c^{\parallel}$ (eV) [5]	−9.5	−12.0
d_1 (eV) [5]	−3.0	−3.0
d_2 (eV) [5]	3.6	3.6
d_3 (eV) [5]	8.82	9.6
d_4 (eV) [5]	−4.41	−4.8
d_5 (eV) [5]	−4.0	−4.0
α_Θ(10^{-4} eV K^{-1})	10.4 [63]	20.5 [87]
β_Θ (K)	1100 [63]	1479 [87]

tables 1 and 2. The values of lattice mismatch for GaN/AlN QD systems are: $\varepsilon_a^* = -2.47\%$ and $\varepsilon_c^* = -4.07\%$, whereas for the CdSe/CdS QD systems they are: $\varepsilon_a^* = -3.99\%$ and $\varepsilon_c^* = -3.87\%$. The calculated values of electromechanical quantities at $(r, z) = (0, 0)$ are given in table 3 for direct comparison. The results of the bandstructure calculations at different temperatures are also presented for truncated conically shaped GaN/AlN QDs.

All our numerical experiments have been performed under the condition for the relative errors between successive refinements to be less than 10^{-6}. In our case it has been achieved with around 10^5 triangular elements. Numerical solutions reflect the effect of the decreasing computational error when the solution approaches the boundary of the domain. Our results in figures 2–5 clearly depict this feature.

3.1. GaN/AlN and CdSe/CdS: cylindrical QDs without WL

First, we report results for cylindrical GaN/AlN and CdSe/CdS QDs without WL. These QDs have a radius of 4 nm and a height of 4 nm.

Figure 2 shows the effect of temperature on electromechanical quantities for the cylindrical GaN/AlN QDs without WL. Inside the QD, the magnitude of ε_{rr} (along the z-axis at $r = 0$, figure 2(a)) decreases with an increase in temperature. At the center of the QD the magnitudes are ∼0.65% at 0 K and ∼0.4% at 1000 K. The magnitude of ε_{rr} decreases towards zero (unstrained region) faster at higher temperature than at lower temperature. As seen from figure 2(b), ε_{zz} is negative everywhere for all temperatures except for the case of 0 K, where near the edges of the QD it takes positive values. The magnitude of ε_{zz} at the center of the QD, i.e. at $z = 0$, is ∼0.18% at 0 K, which increases with an increase in temperature to ∼0.475% at 1000 K. The potential difference across the top and bottom of the QD decreases with an increase in temperature, from ∼2.45 V at 0 K to ∼2.2 V at 1000 K (figure 2(c)). The electric field component E_z exceeds ∼6 MV cm^{-1} near the edges of the QD (figure 2(d)). Inside the QD, the E_z decreases with an increase in temperature, for example, at the center of the QD, E_z = ∼6 MV cm^{-1} at 0 K and E_z = ∼5 MV cm^{-1} at 1000 K. Our results at 300 K are in excellent agreement with recent theoretical [19, 58, 59] and experimental [30] reports.

Figure 3 shows the effect of temperature on the electromechanical quantities for cylindrical CdSe/CdS QDs without WL. Quantities ε_{rr} (figure 3(a)), ε_{zz} (figure 3(b)),

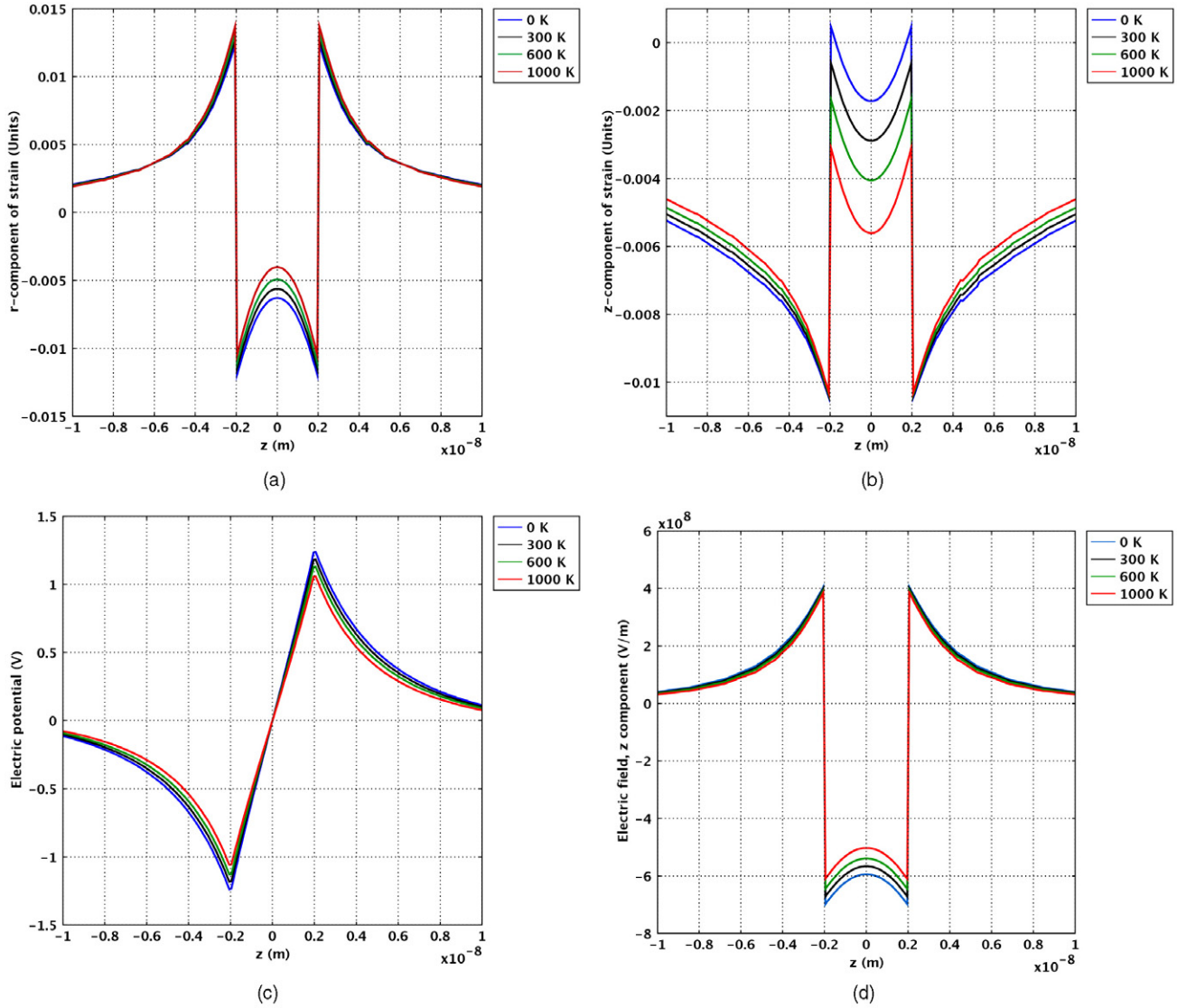

Figure 2. Effect of temperature on electromechanical quantities for cylindrical GaN/AlN QDs without WL. (a) Strain, ε_{rr}, (b) strain, ε_{zz}, (c) electric potential, V, (d) electric field, E_z.

Table 3. Electromechanical parameters at $(r, z) = (0, 0)$ for GaN/AlN QD systems.

Electromechanical parameters	Cylindrical without WL		Cylindrical with WL		Conical truncated with WL	
	$\theta = 0$ K	$\theta = 1000$ K	$\theta = 0$ K	$\theta = 1000$ K	$\theta = 0$ K	$\theta = 1000$ K
ε_{rr} (%)	0.65	0.4	0.65	0.4	1.05	0.8
ε_{zz} (%)	0.18	0.475	0.36	0.73	0.12	0.5
V (V)	2.45	2.2	3.1	2.65	3.4	3.0
E_z (MV cm^{-1})	6.0	5.0	5.8	4.9	6.7	5.8

V (figure 3(c)) and E_z (figure 3(d)) show similar qualitative behavior as their equivalents for GaN/AlN. The magnitudes of ε_{rr}, V and E_z are much smaller, while the magnitude of ε_{zz} is much higher, as compared to those of GaN/AlN. Following are the values of respective electromechanical quantities at the center of the CdSe/CdS QD:

ε_{rr}: at 0 K, ∼0.3% and at 1000 K, ∼0.05%

ε_{zz}: at 0 K, ∼1.2% and at 1000 K to ∼0.95%

V: at 0 K, ∼0.62 V and at 1000 K to ∼0.60 V

E_z: at 0 K, ∼1.3 MV cm^{-1} and at 1000 K to ∼1.35 MV cm^{-1}.

As expected, all the electromechanical quantities exhibit perfect symmetry in cylindrical QDs without WL. The electromechanical parameters for the GaN/AlN QD system are much more sensitive to temperature than their equivalents for CdSe/CdS. This can be attributed to the low values of stress–temperature coefficients (β_i) and relatively weak electromechanical coupling in CdSe/CdS. The only difference

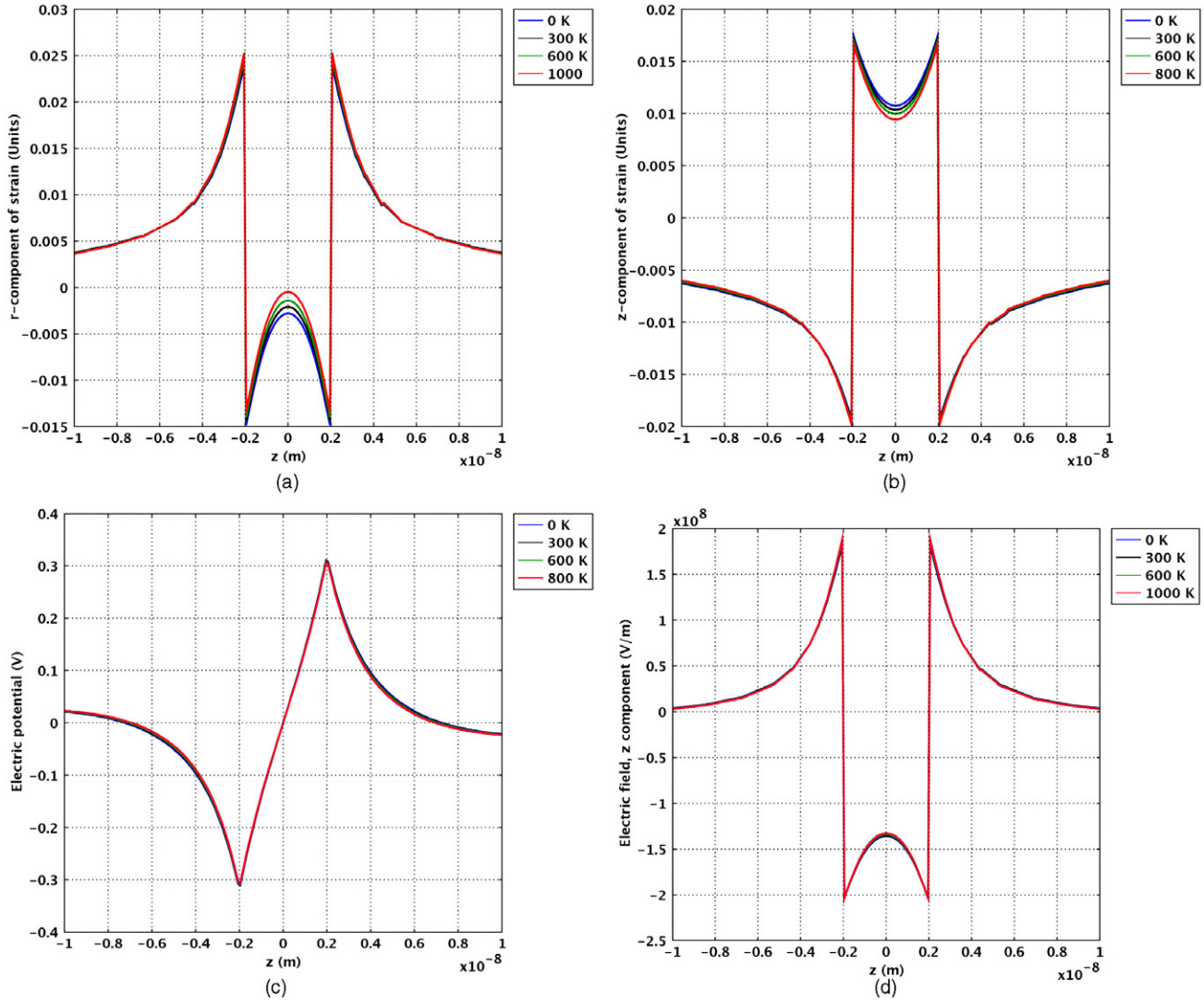

Figure 3. Effect of temperature on electromechanical quantities for cylindrical CdSe/CdS QDs without WL. (a) Strain, ε_{rr}, (b) strain, ε_{zz}, (c) electric potential, V, (d) electric field, E_z.

in the influence of temperature effects on electromechanical quantities in the CdSe/CdS system is quantitative and even that is too small, whereas, in the case of GaN/AlN all electromechanical quantities vary significantly with temperature. Therefore, based on this observation, next we proceed to the study of QDs with WL and different geometries, focusing exclusively on GaN/AlN QDs.

3.2. GaN/AlN: cylindrical QDs with WL

Figure 4 shows the effect of temperature on electromechanical quantities for cylindrical GaN/AlN QDs with WL. The WL is 1 nm thick, while other dimensions of the structure are the same as those in the case without WL.

Very similar values of ε_{rr} (figure 4(a)) are observed in both cases where we consider the GaN/AlN QD with and without WL, except for the WL region, where the difference in values is ∼0.5%. However, values of ε_{zz} (figure 4(b)) are observed to be much higher in the case with WL compared to those values obtained in the case of the QD without WL. In the case of the QD with WL, the value of ε_{zz} is almost doubled compared to the case of the QD without WL. Higher values of strain signify that the structure with WL is less relaxed than the structure without WL. With inclusion of the WL, the potential difference across the ends of the QD increases, while E_z decreases (except for the WL region, where E_z = ∼7 MV cm^{-1}). Accounting for WL provides an additional region in the structure. The resultant geometry becomes asymmetric about the r-axis, which is clearly reflected in our results. Similar strain profiles for QDs with WL are reported in [58, 59].

The qualitative effect of temperature on electromechanical quantities, with (figure 4) and without WL (figure 2) is similar for both geometries analyzed here. We also note that the WL presence hardly modifies the strain component values in zincblende materials [68]. In contrast to this, we observe significantly modified values of ε_{zz} in wurtzite GaN/AlN QDs. This difference in strain behavior can be attributed to the relatively prominent piezoelectric nature of wurtzite materials, which provides an additional degree of freedom for

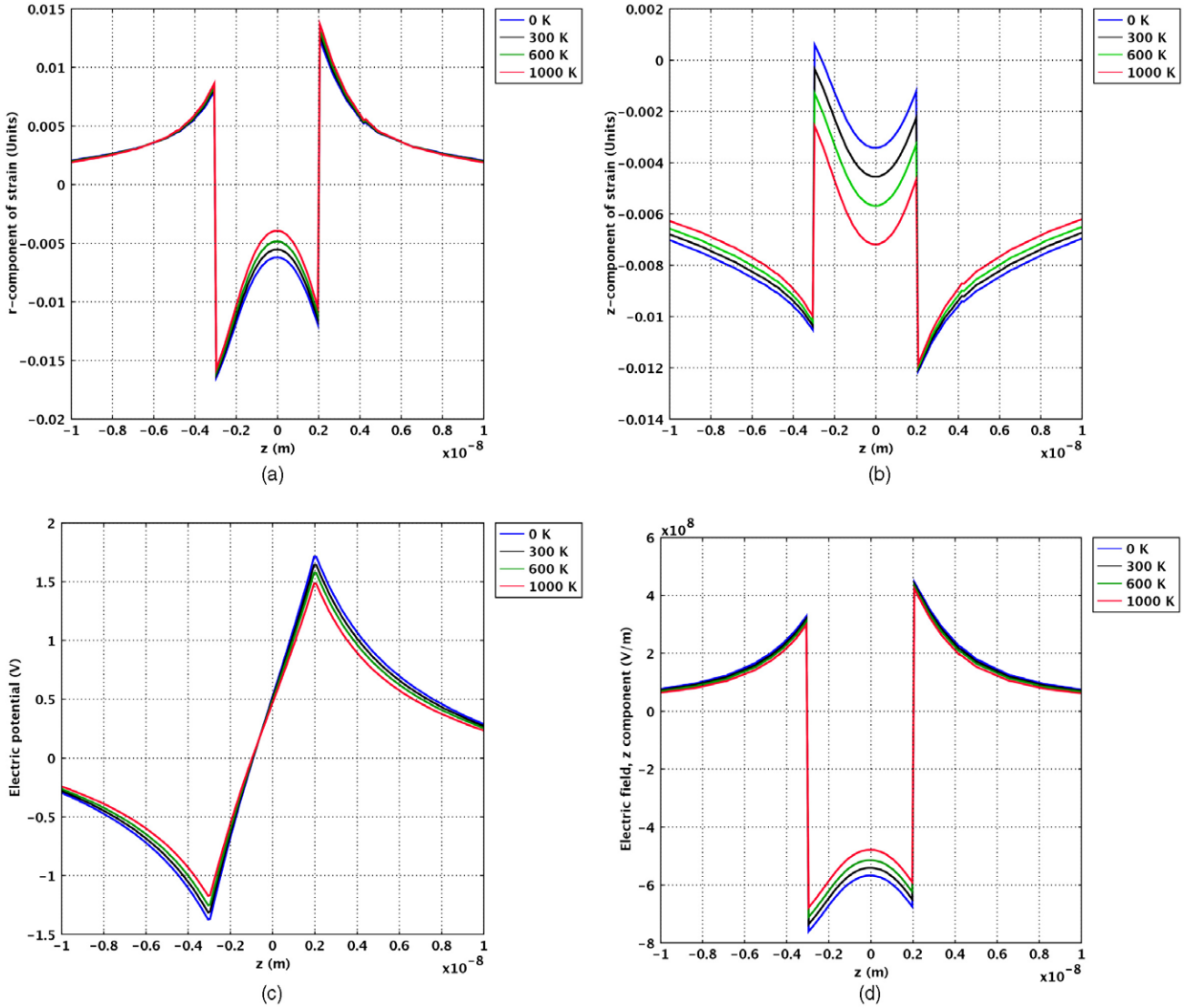

Figure 4. Effect of temperature on electromechanical quantities for cylindrical GaN/AlN QDs with WL. (a) Strain, ε_{rr}, (b) strain, ε_{zz}, (c) electric potential, V, (d) electric field, E_z.

electromechanical loadings to relax. Hence, we conclude that the WL effect on electromechanical quantities significantly differs in zincblende and wurtzite materials. Earlier it has been demonstrated that the ground eigenstate of the entire structure can be considerably affected by the presence of the WL [31]. This indicates that further studies of thermoelectromechanical effects in QDs with WL could be an important avenue of research.

3.3. GaN/AlN: truncated conical QDs with WL

Figure 5 shows the effect of temperature on electromechanical quantities for truncated conical GaN/AlN QDs with WL. The WL is 1 nm thick and the top radius, the bottom radius and the height of the QDs under consideration are 4 nm, 8 nm and 4 nm, respectively.

The magnitudes of the electromechanical quantities are given in table 3 for direct comparison of the values for different geometries of the GaN/AlN QDs. As the temperature increases the strain values decrease rapidly from peak values at edges on either side of the QD. The magnitudes of ε_{rr}, V and E_z are found to decrease with temperature, while ε_{zz} is observed to increase with temperature. The potential difference between the base and the top of QDs creates a deep potential well, for holes at the bottom and for electrons at the top [21]. Thus, the decrease in potential difference with temperature will lead to shallower potential wells, relatively less confinement. A giant built-in electric field of several MV cm^{-1} is a characteristic of GaN/AlN structures and has been observed in several experiments [21, 33, 69] which agrees well with our simulated results (6–8 MV cm^{-1}). Due to this internal electric field, GaN-based LDSNs require relatively higher carrier densities to generate optical gain [33, 70]. Relatively lower carrier densities to generate optical gain may be expected at higher temperatures as our results indicate a decrease in this internal electric field with an increase in temperature.

The highest magnitude of strain tensor component at 0 K, ε_{rr} at $z = 0$, among studied structures of GaN/AlN is about 1%, which is observed in the case of the truncated conical

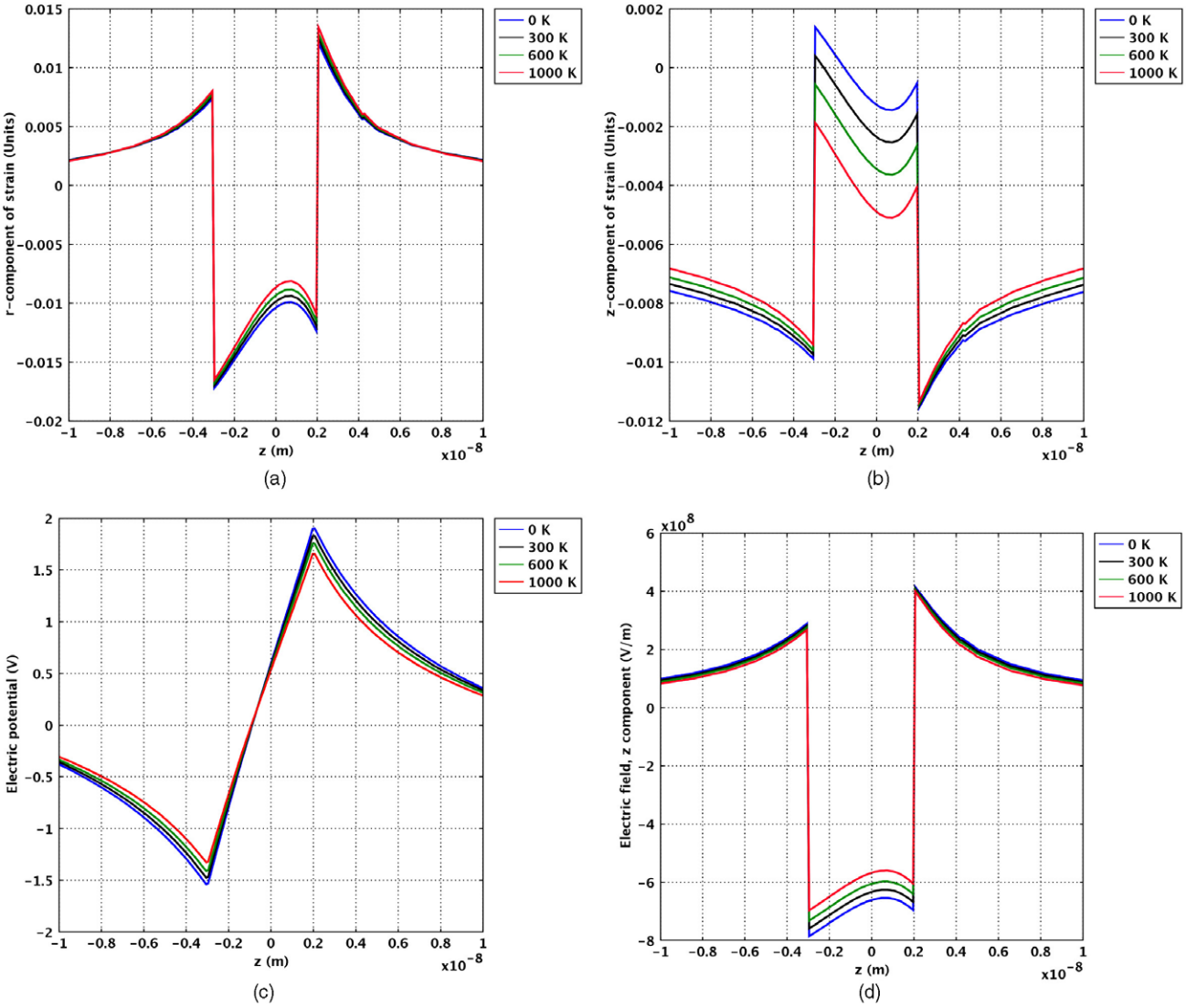

Figure 5. Effect of temperature on electromechanical quantities for truncated conical GaN/AlN QDs with WL. (a) Strain, ε_{rr}, (b) strain, ε_{zz}, (c) electric potential, V, (d) electric field, E_z.

QDs, whereas ε_{zz} takes its maximum value of ∼0.36% in the case of the cylindrical QDs with WL. The potential difference and electric field take their highest magnitudes at 0 K which are ∼3.4 V and ∼6.7 MV cm^{-1}, respectively, for the case of truncated conical QDs.

3.4. GaN/AlN QDs: bandstructure

Most of the electromechanical quantities take higher values and show a significant variation with temperature for truncated conical GaN/AlN QDs with WL. Hence, in order to analyze this issue further, wavefunctions for the ground state and first excited state for truncated conical GaN/AlN QDs with WL under different thermoelectromechanical loadings are calculated using an 8-band $\mathbf{k}\cdot\mathbf{p}$ model and are presented in figures 6 and 7. The significant influence of the WL on the wavefunctions of the QD is discussed in our previous work [31, 32]. In the absence of any thermoelectromechanical loadings we observe the localization at the center of the QDs with the ground state energy, E_1, at about 4.343 236 eV and with the first excited state E_2 = 4.378 34 eV (figures 6(a) and (b)) [31, 32]. However, the electrons are pushed to the QD top when piezoelectric effects are taken into account. This is due to the significantly higher magnitudes of the electric potential and the nature of its profile (figure 5(c)) [5, 20]. The ground state and excited state energies are increased when the piezoelectric effects on bandstructure are taken into account (figures 6(c) and (d)). This effect was experimentally observed through magneto-tunneling spectroscopy measurements that allow the mapping of the electron wavefunctions [71] and was also theoretically proved [72]. The lowest state energies are, $E_1 = 4.373\,267$ eV and $E_2 = 4.418\,84$ eV. These results are in agreement with previous reports on similar geometries [5, 33].

In order to demonstrate the effect of the thermal loading, we present the ground state and first excited states of the electronic system for T = 600 and 1000 K cases in figure 7. The qualitative behavior of electron localizations is dominated by the piezoelectric potentials even at higher temperatures.

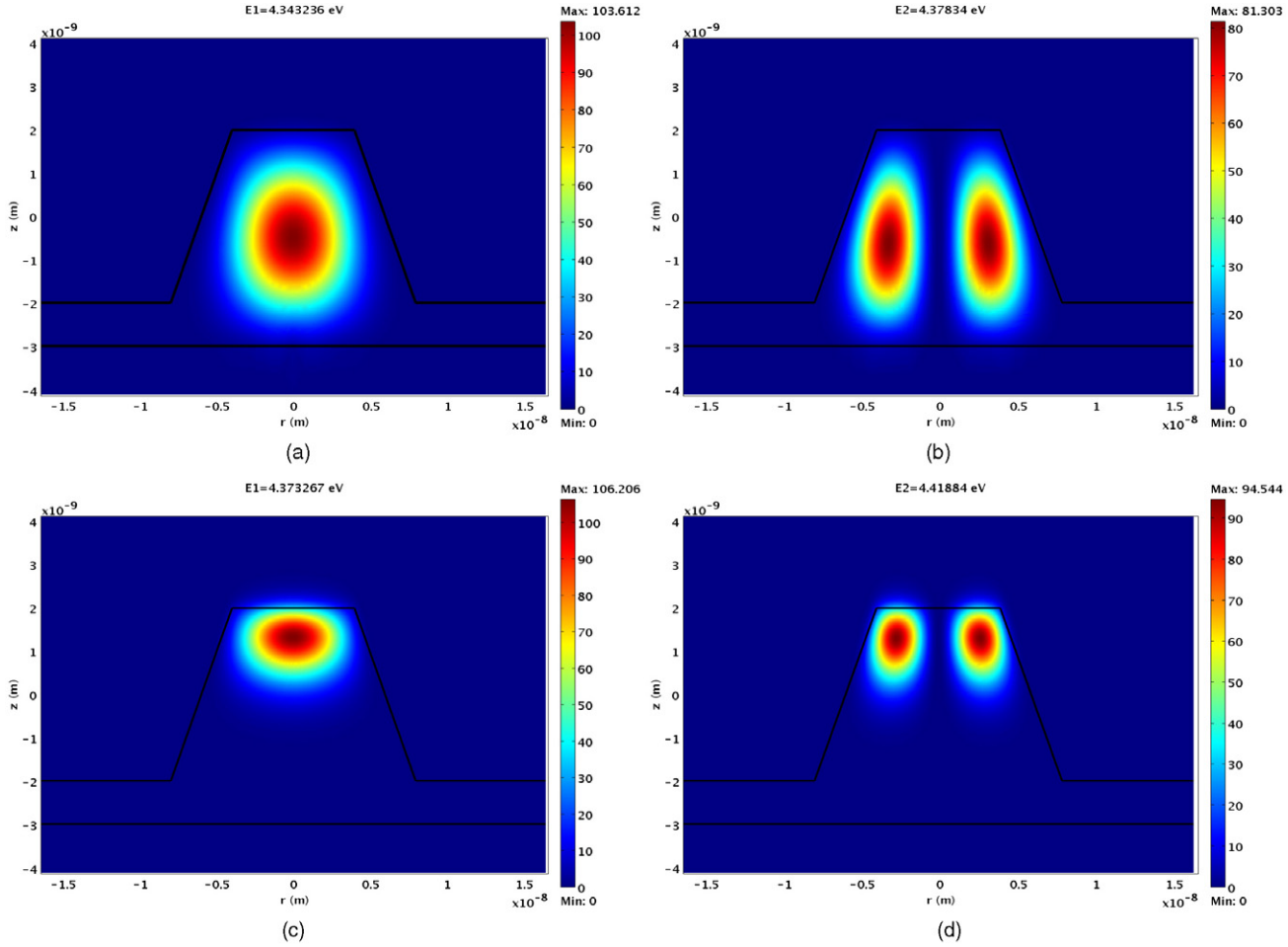

Figure 6. The influence of electromechanical effects on the bandstructure of truncated conical GaN/AlN QDs with WL. (a) Ground state energy E_1 without thermopiezoelectric effects, (b) first excited state energy E_2 without thermopiezoelectric effects, (c) ground state energy E_1 with piezoelectric effects, (d) first excited state energy E_2 with piezoelectric effects.

This is due to the fact that thermal loadings do not change the qualitative profiles of the electromechanical quantities and hence electron localization remains the same as in the case of the bandstructure with piezoelectric effects taken into account. The lowest state energies of the electronic system have been significantly reduced as compared to the case without accounting for temperature effects. This results in subband energies having rigid shifts due to the thermal loadings. The lowest state energies at $T = 600$ K are, $E_1 = 4.254\,236$ eV and $E_2 = 4.295\,872$ eV (figures 7(a) and (b)). At $T = 1000$ K qualitatively localization remains the same, while further reduced lowest state energies are observed, $E_1 = 4.039\,266$ eV and $E_2 = 4.077\,852$ eV (figures 7(c) and (d)). Note that the eigen-energies of electronic states are increased when piezoelectric effects are accounted for and are decreased when thermal loadings are accounted for. Therefore, there could be a situation where these loadings nullify each other's effects on eigen-energies of electronic states. In the present case it can be observed below 600 K. A significant reduction in energies of the electronic states highlights the importance of taking into account operating temperature contributions in the analysis of the QD-based electronic/optoelectronic devices [33] and other applications of QDs.

4. Conclusions

In this study, based on a fully coupled multi-physics model, we have analyzed for the first time combined contributions of thermoelectromechanical effects in GaN/AlN and CdSe/CdS QDs with different geometries, accounting for the WL. It has been found that GaN/AlN QD systems (III–V group semiconductors) are more sensitive to thermal loadings compared to CdSe/CdS QD systems (II–VI group semiconductors). Thermal loadings lead to the increase in magnitude of the strain tensor component ε_{rr} and decrease in ε_{zz}. However, the electric potential and the electric field are observed to decrease with increase in temperature. Relatively lower carrier densities to generate optical gain may be expected at higher temperatures. The WL effect on thermoelectromechanical distributions differs significantly in zincblende and wurtzite nanostructures. A significant reduction in electronic state energies due to thermal loadings is observed. Thus, in addition to electromechanical tuning, the operating temperature can also provide an additional tuning parameter in band gap engineering of QDs. However, there could be a situation where electromechanical and thermal loadings may

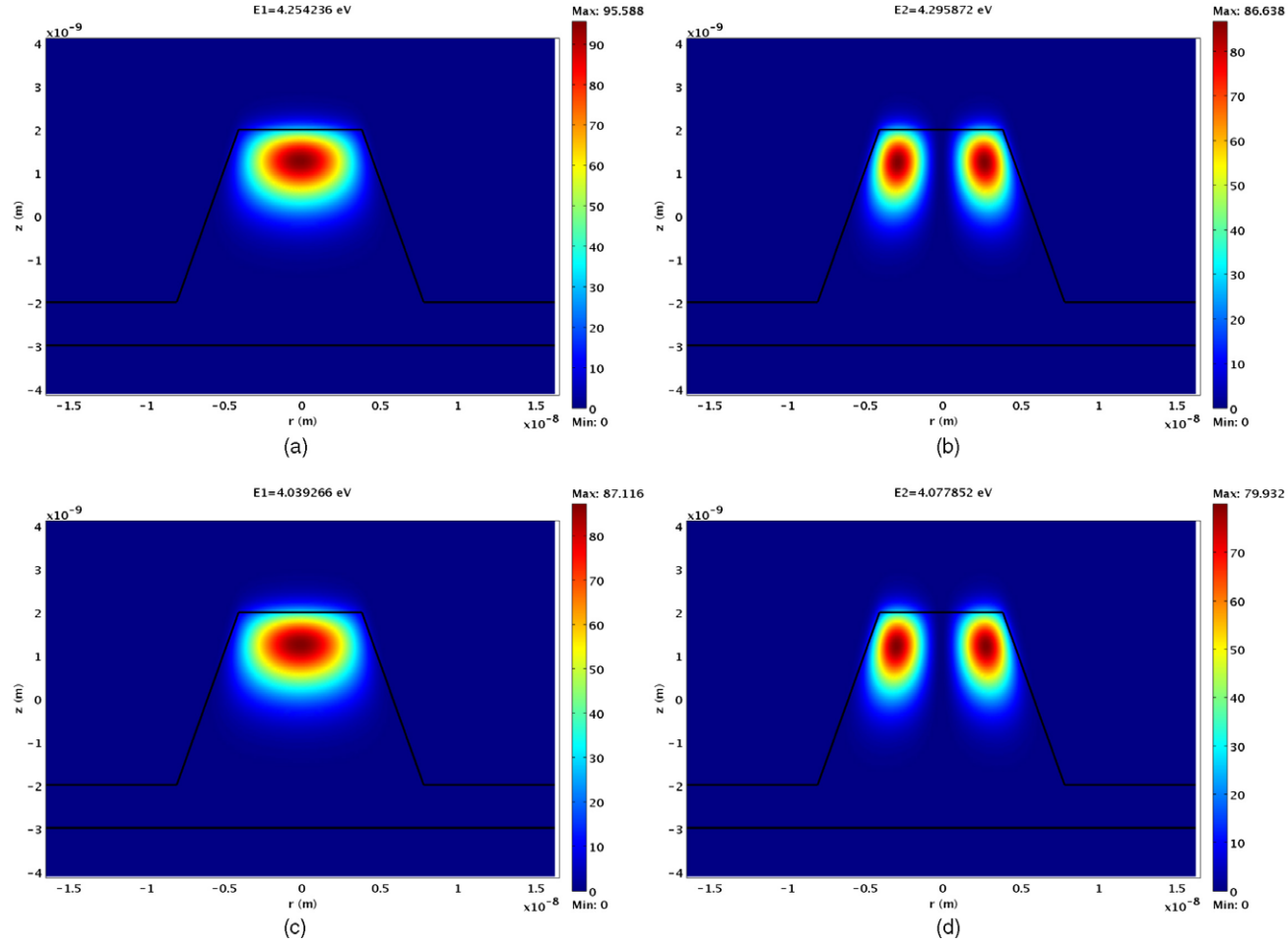

Figure 7. The influence of thermopiezoelectric effects on the bandstructure of truncated conical GaN/AlN QDs with WL. (a) Ground state energy E_1 with thermopiezoelectric effects, $T = 600$ K, (b) first excited state energy E_2 with thermopiezoelectric effects, $T = 600$ K, (c) ground state energy E_1 with thermopiezoelectric effects, $T = 1000$ K, (d) first excited state energy E_2 with thermopiezoelectric effects, $T = 1000$ K.

nullify their effects on eigen-energies of electronic states, making the bandstructures of QDs unaffected in such cases by thermoelectromechanical effects. The observed phenomena emphasize the importance of the fully coupled thermopiezoelectric models in studying the properties of LDSNs, in particular QDs.

Acknowledgments

This work, conducted in the M^{2}NeT Laboratory (http://www.m2netlab.wlu.ca), was made possible by the facilities of the Shared Hierarchical Academic Research Computing Network (SHARCNET). RM acknowledges the support from the NSERC and CRC program.

References

[1] Melnik R and Mahapatra R 2007 *Comput. Struct.* **85** 698–711
[2] Maranganti R and Sharma P 2003 *J. Comput. Theor. Nanosci.* **4** 715–38
[3] Chuang S L 1995 *Physics of Optoelectronic Devices* (New York: Wiley)
[4] Downes J R, Faux D A and O'Reilly E P 1995 *Mater. Sci. Eng.* B **35** 357–63
[5] Fonoberov V A and Balandin A A 2003 *J. Appl. Phys.* **94** 7178–86
[6] Yang R, Chen G and Dresselhaus M S 2005 *Nano Lett.* **5** 1111–5
[7] Yang R, Chen G and Dresselhaus M S 2005 *Phys. Rev.* B **72** 125418
[8] Lin Y M and Dresselhaus M S 2003 *Phys. Rev.* B **68** 075304
[9] Heremans J P, Jovovic V, Toberer E S, Saramat A, Kurosaki K, Charoenphakdee A, Yamanaka S and Snyder G J 2008 *Science* **321** 554–7
[10] Snyder G J and Toberer E S 2008 *Nat. Mater.* **7** 105–14
[11] Ikeda T, Collins L A, Ravi V A, Gascoin F S, Haile S M and Snyder G J 2007 *Chem. Mater.* **19** 763–7
[12] Kulkarni A J and Zhou M 2007 *Nanotechnology* **18** 435706
[13] Liu W and Balandin A A 2005 *J. Appl. Phys.* **97** 123705
[14] Davies J H 2003 *ASME J. Appl. Mech.* **70** 655–60
[15] Melnik R V N 2003 *Math. Comput. Simul.* **61** 497–507
[16] Kamath H, Willatzen M and Melnik R V N 2006 *Ultrasonics* **44** 64–72
[17] Giazotto F, Heikkil T T, Luukanen A, Savin A M and Pekola J P 2006 *Rev. Mod. Phys.* **78** 217–74
[18] Chen X O, Dong B and Lei X L 2008 *Chin. Phys. Lett.* **25** 3032–5
[19] Lassen B, Willatzen M, Barettin D, Melnik R V N and Voon L C 2008 *J. Phys.: Conf. Ser.* **107** 012008

[20] Williams D P, Andreev A D, OReilly E P and Faux D A 2005 *Phys. Rev.* B **72** 235318
[21] Andreev A D and OReilly E P 2000 *Phys. Rev.* B **62** 15851–70
[22] Melnik R V N and He H 2000 *Modelling Simul. Mater. Sci. Eng.* **8** 133–49
[23] Melnik R V N and He H 2000 *Math. Comput. Simul.* **52** 273–87
[24] Melnik R V N and He H 2000 *J. Eng. Math.* **38** 233–63
[25] Melnik R V N and Rimshans J 2003 *Dynamics of Continuous Discrete and Impulsive Systems—Series B, Applications and Algorithms* (Suppl. S) (Ontario: Watam Press) pp 102–7
[26] Radulovic N, Willatzen M and Melnik R V N 2004 *Computational Science and its Applications—ICCSA 2004* (*Lecture Notes in Computer Science* vol 3045 PT 3) ed A Lagana *et al* (Berlin: Springer-Verlag) pp 817–26
[27] Radulovic N, Willatzen M, Melnik R V N and Voon L C L Y 2006 *J. Comput. Theor. Nanosci.* **3** 551–9
[28] Moreira S G C, Silva E C da, Mansanares A M, Barbosa L C and Cesar C L 2007 *Appl. Phys. Lett.* **91** 021101
[29] Wen B and Melnik R V N 2008 *Appl. Phys. Lett.* **92** 261911
[30] Arley M, Rouviere J L, Widmann F, Daudin B, Feuillet G and Mariette H 1999 *Appl. Phys. Lett.* **74** 3287–9
[31] Melnik R V N and Willatzen M 2004 *Nanotechnology* **15** 1–8
[32] Melnik R V N and Zotsenko K N 2004 *Modelling Simul. Mater. Sci. Eng.* **12** 465–77
[33] Grandjean N and Ilegems M 2007 *Proc. IEEE* **95** 1853
[34] Melnik R V N 2001 *Comput. Phys. Commun.* **142** 231–7
[35] Melnik R V N 2003 *Int. Commun. Heat Mass Transfer* **30** 83–92
[36] Melnik R V N 2000 *Appl. Math. Comput.* **107** 27–55
[37] Melnik R V N 1997 *Math. Mech. Solids* **2** 153–80
[38] Melnik R V N and Melnik K N 1998 *Commun. Numer. Methods Eng.* **14** 839–47
[39] Melnik R V N 1998 *J. Differ. Eqns Appl.* **4** 185–212
[40] Melnik R V N and Melnik K N 2000 *Appl. Math. Model.* **24** 147–63
[41] Melnik R V N and Zotsenko K N 2004 *Appl. Numer. Math.* **48** 41–62
[42] Bahrami-Samani M and Melnik R V N 2008 *Appl. Phys. Lett.* submitted
[43] Bies W E, Radtke R J and Ehrenreich H 2002 *Phys. Rev.* B **65** 085208
[44] Melnik R V N and Roberts A J 2001 *J. Physique* IV **11** 515–20
[45] Perez-Aparicio J L, Taylor R L and Gavela D 2007 *Comput. Mech.* **40** 35–45
[46] Melnik R V N 2001 *Appl. Math. Comput.* **122** 107–32
[47] Strunin D V, Melnik R V N and Roberts A J 2001 *J. Therm. Stresses* **24** 121–40
[48] Melnik R V N and Roberts A J 2003 *Z. Angew. Math. Mech.* **83** 93–104
[49] Matus P, Melnik R V N, Wang L and Rybak I 2004 *Math. Comput. Simul.* **65** 489–509
[50] Melnik R V N, Strunin D V and Roberts A J 2005 *Numer. Heat Transfer* A **47** 549–69
[51] Wang L and Melnik R V N 2006 *Appl. Math. Mech.* **27** 1185–96
[52] Patil S and Melnik R V N 2009 in preparation
[53] Lassen B, Willatzen M and Melnik R 2006 *J. Comput. Theor. Nanosci.* **3** 588–97
[54] Yamamoto A and Yamaguchi S 2004 *Mater. Res. Soc. Symp. Proc.* **793** S8.24.1
[55] Kaiwa N, Hoshino M, Yaginuma T, Izaki R, Yamaguchi S and Yamamoto A 2007 *Thin Solid Films* **515** 4501–4
[56] Nan C W 1994 *Phys. Rev.* B **49** 12619–24
[57] Barettin D, Lassen B and Willatzen M 2008 *J. Phys.: Conf. Ser.* **107** 012001
[58] Andreev A D and OReilly E P 2000 *Nanotechnology* **11** 25662
[59] Andreev A D and OReilly E P 2001 *Physica* E **10** 55360
[60] Melnik R V N 2000 *Eng. Comput.* **17** 386–416
[61] Lassen B, Melnik R V N and Willatzen M 2009 *Commun. Comput. Phys.* at press
[62] Lassen B, Willatzen M, Melnik R and Voon L C L Y 2005 *J. Math. Phys.* **46** 112102
[63] Wang J Z, Huang P J, Huang Y S, Firszt F, Legowski S, Meczynska H, Marasek A and Tiong K K 2007 *J. Phys.: Condens. Matter* **19** 096216
[64] Nakaoka T, Kako S and Arakawa Y 2006 *Physica* E **32** 148–51
[65] Lassen B, Willatzen M, Melnik R and Voon L C L Y 2006 *J. Mater. Res.* **21** 2927–35
[66] Zhang J C, Meyler B, Vardi A, Bahir G and Salzman J 2008 *J. Appl. Phys.* **104** 044307
[67] Daudin B, Widmann F, Feuillet G, Samson Y, Arlery M and Rouviere J L 1997 *Phys. Rev.* B **56** R7069
[68] Lee S, Lazarenkova O L, Allmen P V, Oyafuso F and Klimeck G 2004 *Phys. Rev.* B **70** 125307
[69] Grandjean N, Leroux M and Massies J 1999 *Appl. Phys. Lett.* **74** 2361–3
[70] Bernardini F, Fiorentini V and Vanderbilt D 1997 *Phys. Rev.* B **56** R10024-7
[71] Patanè A *et al* 2002 *Phys. Rev.* B **65** 165308
[72] Migliorato M A, Powell D, Liew S L, Cullis A G, Navaretti P, Steer M J, Hopkinson M, Fearn M and Jefferson J H 2004 *J. Appl. Phys.* **96** 5169–72
[73] Fonoberov V and Balandin A 2004 *J. Vac. Sci. Technol.* B **22** 2190–4
[74] Madelung O 2004 *Semiconductors: Data Handbook* 3rd edn (Berlin: Springer)
[75] Iwanaga H, Kunishige A and Takeuchi S 2000 *J. Mater. Sci.* **35** 2451–4
[76] Zaika G A 1994 *J. Math. Sci.* **68** 688–9
[77] Ninomiya S and Adachi S 1995 *J. Appl. Phys.* **78** 1183–90
[78] Adachi S 2004 *Handbook on Physical Properties of Semiconductors* (Norwell: Kluwer–Academic)
[79] Chang Y, Tong K Y and Surya C 2005 *Semicond. Sci. Technol.* **20** 188–92
[80] Liu S T and Long D 1978 *Proc. IEEE* **66** 14–26
[81] Manasreh M O 2000 *Optoelectronic Properties of Semiconductors and Superlattices* vol 7 *GaN and Related Materials* ed S J Pearton (Boca Raton, FL: CRC Press)
[82] Levinshtein M E, Rumyantsev A L and Shur M S (ed) 2001 *Properties of Advanced Semiconductor Materials: GaN, AlN, InN, BN, SiC, SiGe* (New York: Wiley)
[83] Gerlich D, Dole S L and Slack G A 1986 *J. Phys. Chem. Solids* **47** 437–41
[84] Thokala R and Chaudhuri J 1995 *Thin Solid Films* **266** 189–91
[85] Dutta M, Brown G J, Ramadurai D, Geerpuram D, Yang J, Kohanpour B, Chen C and Stroscio M A 2005 *Nonequilibrium Carrier Dynamics in Semiconductors: Proc. 14th Int. Conf. (Chicago)* (*Springer Proceedings in Physics*) (Berlin: Springer)
[86] Ahmad I, Holtz M, Faleev N N and Temkin H 2004 *J. Appl. Phys.* **95** 1692–7
[87] Iwata S, Nanjoa Y, Okunoa T, Kuraia S and Taguchia T 2007 *J. Cryst. Growth* **301** 461–4